Interplay of charge and orbital ordering in manganese perovskites

K. H. Ahn and A. J. Millis
Department of Physics and Astronomy, The Johns Hopkins University, Baltimore, Maryland 21218
(Received 17 February 1998)

A model of localized classical electrons coupled to lattice degrees of freedom and, via the Coulomb interaction, to each other has been studied to gain insight into the charge and orbital ordering observed in lightly doped manganese perovskites. Expressions are obtained for the minimum energy and ionic displacements caused by given hole and electron orbital configurations. The expressions are analyzed for several hole configurations, including that experimentally observed by Yamada *et al.* [Phys. Rev. Lett. **77**, 904 (1996)] in $La_{7/8}Sr_{1/8}MnO_3$. We find that, although the preferred charge and orbital ordering depend sensitively on parameters, there are ranges of the parameters in which the experimentally observed hole configuration has the lowest energy. For these parameter values we also find that the energy differences between different hole configurations are on the order of the observed charge ordering transition temperature. The effects of additional strains are also studied. Some results for $La_{1/2}Ca_{1/2}MnO_3$ are presented, although our model may not adequately describe this material because the high-temperature phase is metallic. [S0163-1829(98)01431-3]

Over the past few years much attention has been focused on manganese perovskite-based oxides, most notably the pseudocubic materials $R_{1-x}A_xMnO_3$. (Here R is a rare earth element such as La and A is a divalent alkali metal element such as Ca or Sr.) The initial motivation came from the observation that for some range of x and temperature T, resistance can be reduced by a factor of up to 10^7 in the presence of a magnetic field.[1] Two other interesting physical phenomena occurring in this class of materials are charge ordering and orbital ordering.[2] In this paper we study the connection between the two.

The important electrons in $R_{1-x}A_xMnO_3$ are the Mn e_g electrons; their concentration is $1-x$. For many choices of R, A, and x, especially at commensurate x values, the e_g charge distribution is not uniform and it indeed appears that a fraction x of Mn ions have no e_g electron while $1-x$ have a localized e_g electron. A periodic pattern of filled and empty sites is said to exhibit charge ordering. There are two e_g orbitals per Mn ion. A localized Mn e_g electron will be in one linear combination of these; a periodic pattern of orbital occupancy is said to exhibit orbital ordering. Recently, Murakami *et al.*[3] observed the charge ordering transition accompanying simultaneous orbital ordering in $La_{1/2}Sr_{3/2}MnO_4$ at 217 K (well above the magnetic phase transition temperature 110 K). It indicates that the interplay of the charge and orbital ordering to minimize the lattice energy could be the origin of the charge ordering. In this paper we present an expression for the coupling between charge and orbital ordering, with different charge ordering patterns favoring different orbital orderings. We also argue that the orbital ordering energy differences determine the observed charge ordering in lightly doped manganites. Localized charges induce local lattice distortions, which must be accommodated into the global crystal structure; the energy cost of this accommodation is different for different charge ordering patterns.

To model the charge and orbital ordering, we assume that the electrons are localized classical objects, so that each Mn site is occupied by zero or one e_g electron and each e_g electron is in a definite orbital state. This assumption seems reasonable in the lightly doped materials such as $La_{7/8}Sr_{1/8}MnO_3$, which are strongly insulating at all temperatures,[4] but may not be reasonable for the $La_{1/2}Ca_{1/2}MnO_3$ composition,[2] where the charge ordered state emerges at a low temperature from a metallic state. We proceed by calculating the energies of different charge ordering patterns, emphasizing the 1/8 doping case. It is practically impossible to consider all possible charge ordering configurations. Therefore, we consider the three configurations shown in Fig. 1, which are the only ones consistent with the following basic features of the hole lattice implied by the experimental results by Yamada *et al.*:[4] invariance under translation by two lattice constants in the x or y direction, four in the z direction, and an alternating pattern of occupied and empty planes along the z direction. The configuration in Fig. 1(b) is the one proposed by Yamada *et al.*[4] to explain their experimental results for $La_{7/8}Sr_{1/8}MnO_3$. For localized electrons there are three energy terms: the coupling to the lattice, which will be discussed at length below, the Coulomb interaction, and the magnetic interaction.

First, we argue that the Coulomb energy cannot explain the observed ordering pattern or transition temperature. We take as a reference the state with one e_g electron per Mn and

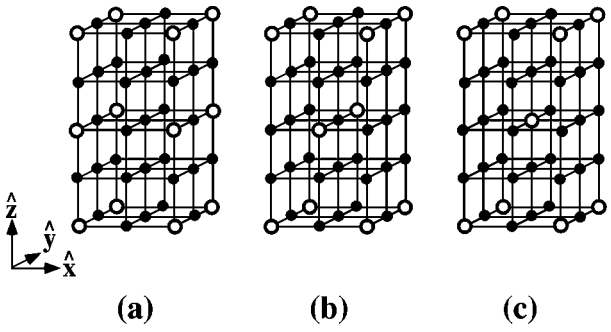

FIG. 1. Three hole ordering patterns for $R_{7/8}A_{1/8}MnO_3$ considered in our calculations. Solid circles represent Mn^{3+}, and open circles Mn^{4+}.

denote by δq_i the charge of a hole on a Mn site. From the classical Coulomb energy

$$U_{\text{Coulomb}}=\frac{1}{2\epsilon_0}\sum_{i\neq j}\frac{\delta q_i \delta q_j}{r_{ij}} \tag{1}$$

one finds that the difference in energy between the configurations in Fig. 1 is

$$\Delta\mathcal{U}_{\text{Coulomb, per hole}}=\frac{1}{2\epsilon_0}\sum_{i\neq 0}\frac{\Delta(\delta q_i)}{r_{i0}}, \tag{2}$$

where 0 is a site containing a hole and $\Delta(\delta q)$ is the difference in charge between the two configurations. We estimated the above infinite sum by repeated numerical calculations for larger and larger volumes of the unit cells around the origin. We find that Fig. 1(c) has the lowest energy, $12\ \text{meV}/\epsilon_0$ lower than Fig. 1(b) and $27\ \text{meV}/\epsilon_0$ lower than Fig. 1(a).

To estimate the magnitude of the Coulomb energy differences, we need an estimate for the dielectric constant ϵ_0, which we obtain from the measured reflectivity for $La_{0.9}Sr_{0.1}MnO_3$ (Ref. 5) and the Lyddane-Sachs-Teller relation[6] $\omega_L^2=\omega_T^2\epsilon_0/\epsilon_\infty$. At frequencies greater than the greatest phonon frequency the reflectivity is close to 0.1, implying $\epsilon_\infty\approx 3.4$; the reflectivity is near unity between $\omega_T=0.020$ eV and $\omega_L=0.024$ eV, implying $\epsilon_0\approx 5.0$. Because both $La_{7/8}Sr_{1/8}MnO_3$ and $La_{0.9}Sr_{0.1}MnO_3$ are insulating and have similar compositions, their static dielectric constants are expected to be similar. Using $\epsilon_0\approx 5.0$, the energy difference between different configurations of holes is only around 2.4 meV, or 30 K per hole, which is small compared to the observed charge ordering temperature of 150–200 K of these materials. The inconsistency with the experimentally observed hole configuration and the smallness of the energy difference scale indicate that the electrostatic energy is not the main origin of charge ordering for this material.

Even though the magnetic and charge ordering transitions show a correlation in $La_{7/8}Sr_{1/8}MnO_3$,[7] we do not think that the magnetic contribution to charge and orbital ordering is as important as the lattice contribution for three reasons. First, in undoped $LaMnO_3$, the orbital ordering and the structural phase transition occur at around 800 K and the magnetic ordering at around 140 K,[8,9] suggesting that the magnetic effects are relatively weak. Second, in $La_{7/8}Sr_{1/8}MnO_3$ the Mn spins are ferromagnetically ordered with the moment close to the full Mn moment at temperatures greater than the charge ordering temperature[7] and ferromagnetic order does not favor one charge configuration over another. Third, although in $La_{7/8}Sr_{1/8}MnO_3$ antiferromagnetic order appears at the charge ordering transition, the antiferromagnetic moment is very small (less than 0.1 of the full Mn moment),[7] so the energy associated with this ordering must be much less than 140 K/site associated with magnetic ordering in $LaMnO_3$. Therefore, we think that the canted antiferromagnetism occurring upon charge ordering in $La_{7/8}Sr_{1/8}MnO_3$ (Ref. 7) is not the cause but the effect of the charge and orbital ordering. We now turn our attention to the lattice energy.

A classical model for the lattice distortions of the insulating perovskite manganites has been derived in Ref. 10 and shown to be consistent with experimental results on $LaMnO_3$. This model is adopted here with an additional term, an energy cost for shear strain. We now briefly outline the model, which is explained in more detail in Ref. 10 and the Appendix. The ionic displacements included are the vector displacement $\vec{\delta}_i$ of the Mn ion on site i and the $\hat{a}$ directional scalar displacement u_i^a ($a=x,y$, and z) of the O ion, which sits between the Mn ion on site i and the Mn ion on site $i+\hat{a}$. For convenience, $\vec{\delta}_i$ and u_i^a are defined to be dimensionless in the following way: The lattice constant of the ideal cubic perovskite is b, the Mn ion position in the ideal cubic perovskite is $\vec{R}_i$, the actual Mn ion position is $\vec{R}_i+b\vec{\delta}_i$, and the actual O ion position is $\vec{R}_i+(b/2+bu_i^a)\hat{a}$. The lattice energy is taken to be harmonic and depends only on the nearest neighbor Mn-O distance and the first and second nearest neighbor Mn-Mn distances. The spring constants corresponding to these displacements are K_1,K_2, and K_3, as shown in Fig. 2. Because K_1 and K_2 involve bond stretching while K_3 involves bond bending, $K_1\geqslant K_2\gg K_3$ is expected. Thus $E_{\text{lattice}}=E_{\text{Mn-O}}+E_{\text{Mn-Mn, first}}+E_{\text{Mn-Mn, second}}$, where

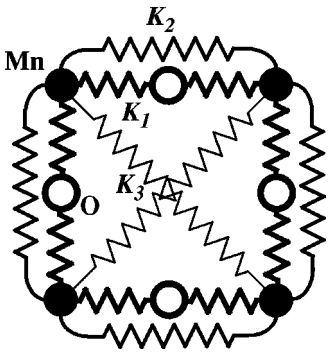

FIG. 2. Spring constants: K_1 between the nearest neighbor Mn-O, K_2 between the first neighbor Mn-Mn, and K_3 between the second neighbor Mn-Mn.

$$E_{\text{Mn-O}}=\frac{1}{2}K_1\sum_{i,a}(\delta_i^a-u_i^a)^2+(\delta_i^a-u_{i-a}^a)^2, \tag{3}$$

$$E_{\text{Mn-Mn,first}}=\frac{1}{2}K_2\sum_{i,a}(\delta_i^a-\delta_{i-a}^a)^2, \tag{4}$$

$$E_{\text{Mn-Mn,second}}=\frac{1}{2}K_3\sum_{i,(a,b)}\left[\left(\frac{\delta_{i+a+b}^a+\delta_{i+a+b}^b}{\sqrt{2}}\right)-\left(\frac{\delta_i^a+\delta_i^b}{\sqrt{2}}\right)\right]^2+\left[\left(\frac{\delta_{i+a-b}^a-\delta_{i+a-b}^b}{\sqrt{2}}\right)-\left(\frac{\delta_i^a-\delta_i^b}{\sqrt{2}}\right)\right]^2. \tag{5}$$

In the above equations a denotes x,y, and z, and (a,b) represents $(x,y),(y,z)$, and (z,x). $E_{\text{Mn-Mn, second}}$ was not considered in Ref. 10. The shear modulus produced by this term is important because without it, a Mn ion on site $i+\hat{x}$ can have arbitrary large y directional displacement relative to the Mn ion on site i at no cost of energy. For this reason, the model with $K_3=0$ has singularities, whose proper treatment requires $K_3\neq 0$ in our model. However, still we expect K_3 will be much smaller than K_1 or K_2. Therefore, in order to

simplify the calculation, the $K_3/K_1 \to 0$ limit has been taken after the expression of minimized energy and equilibrium ionic displacements have been obtained.

Second, we consider the electronic degree of freedom. We parametrize the electron density by the variable h_i. If an electron is present on site $i, h_i = 0$; if no electron is present, $h_i = 1$. If there is an electron on site i, the electron orbital state, which is a linear combination of the two e_g orbitals, is parametrized by an angle θ_i as

$$|\psi_i(\theta_i)\rangle = \cos\ \theta_i |d_{3z^2-r^2}\rangle + \sin\ \theta_i |d_{x^2-y^2}\rangle, \tag{6}$$

with $0 \leqslant \theta_i < \pi$. The electron orbital state couples to the distortion of the surrounding oxygen octahedra through the Jahn–Teller distortion. The coupling is given by

$$\begin{aligned} E_{\rm JT} &= -\lambda \sum_i\ (1-h_i)\left[\cos 2\theta_i \left\{ v_i^z - \frac{1}{2}(v_i^x + v_i^y)\right\}\right. \\ &\quad \left. + \sin 2\theta_i \frac{\sqrt{3}}{2}(v_i^x - v_i^y)\right] \\ &= -\lambda \sum_{i,a}\ (1-h_i) v_i^a \cos 2(\theta_i + \psi_a), \end{aligned} \tag{7}$$

where

$$v_i^a = u_i^a - u_{i-a}^a, \tag{8}$$

$$\psi_x = -\pi/3, \quad \psi_y = \pi/3, \quad \psi_z = 0. \tag{9}$$

If a hole is present on site i, it attracts the surrounding oxygen ions equally, giving rise to a breathing distortion energy given by

$$E_{\rm hole} = \beta\lambda \sum_i\ h_i (v_i^x + v_i^y + v_i^z). \tag{10}$$

The parameter β represents the strength of the breathing distortion relative to the Jahn–Teller distortion. Finally, following Kanamori,[9] we include a phenomenological cubic anharmonicity term given by

$$E_{\rm anharm} = -A \sum_i\ (1-h_i)\cos 6\theta_i. \tag{11}$$

The sign has been chosen so that the electron orbital states of $|3x^2-r^2\rangle, |3y^2-r^2\rangle$, or $|3z^2-r^2\rangle$, with $\hat{x}, \hat{y}$, and $\hat{z}$ pointing toward nearest oxygen ions, are favored when A is positive. The total energy, which is the sum of all the above energy terms, is given by

$$\begin{aligned} E_{\rm tot} &= E_{\text{Mn-O}} + E_{\text{Mn-Mn, first}} + E_{\text{Mn-Mn, second}} \\ &\quad + E_{\rm JT} + E_{\rm hole} + E_{\rm anharm}. \end{aligned} \tag{12}$$

We minimized $E_{\rm tot}$ about δ_i^a's and u_i^a's for fixed hole and orbital configurations. These are conveniently expressed in terms of the variables $\delta_{\vec{k}}^a$, $u_{\vec{k}}^a$, $h_{\vec{k}}$, and $c_{\vec{k}}^a$ defined as

$$\delta_i^a = \sum_{\vec{k}}\ e^{-i\vec{k}\cdot\vec{R}_i} \delta_{\vec{k}}^a, \tag{13}$$

$$u_i^a = \sum_{\vec{k}}\ e^{-i\vec{k}\cdot\vec{R}_i} u_{\vec{k}}^a, \tag{14}$$

$$h_i = \sum_{\vec{k}}\ e^{-i\vec{k}\cdot\vec{R}_i} h_{\vec{k}}, \tag{15}$$

$$(1-h_i)\cos 2(\theta_i + \psi_a) = \sum_{\vec{k}}\ e^{-i\vec{k}\cdot\vec{R}_i} c_{\vec{k}}^a. \tag{16}$$

The details are shown in the Appendix. The minimized energy per Mn ion may be written as

$$\frac{E_{\rm tot}}{N} = \mathcal{E}_{\vec{k}=0} + \sum_{\vec{k}\neq 0, a}\ \mathcal{E}_{\vec{k}}^a + \frac{E_{\rm anharm}}{N}, \tag{17}$$

where

$$\mathcal{E}_{\vec{k}}^a = \begin{cases} -\dfrac{\lambda^2}{(K_1+2K_2)K_1}[K_1 + K_2(1-\cos\ k_a)] \\ \quad \times (\beta h_{\vec{k}} - c_{\vec{k}}^a)(\beta h_{-\vec{k}} - c_{-\vec{k}}^a), \quad \text{if } k_a \neq 0 \\ 0 \quad \text{if } k_a = 0, \end{cases} \tag{18}$$

$$\mathcal{E}_{\vec{k}=0} = -\frac{\lambda^2}{K_1+2K_2}\left[3(\beta h_0)^2 + \sum_a\ (c_0^a)^2\right]. \tag{19}$$

The long-wavelength strain e^{ab} and the $\vec{k}(\neq 0)$ components of the ionic displacements are given as

$$e^{ab} = -\frac{2\lambda}{K_1+2K_2}(\beta h_0 - c_0^a)\delta_{ab}, \tag{20}$$

$$u_{\vec{k}\neq 0}^a = \begin{cases} -\dfrac{\lambda[K_1 + K_2(1-\cos\ k_a)]}{(K_1+2K_2)K_1} \dfrac{1-e^{-ik_a}}{1-\cos\ k_a} \\ \quad \times (\beta h_{\vec{k}} - c_{\vec{k}}^a) \quad \text{if } k_a \neq 0 \\ 0 \quad \text{if } k_a = 0, \end{cases} \tag{21}$$

$$\delta_{\vec{k}\neq 0}^a = \begin{cases} -i\ \dfrac{\lambda \sin\ k_a}{(K_1+2K_2)(1-\cos\ k_a)}(\beta h_{\vec{k}} - c_{\vec{k}}^a) & \text{if } k_a \neq 0 \\ 0 & \text{if } k_a = 0. \end{cases} \tag{22}$$

Because h_i's and $(1-h_i)\cos 2(\theta_i + \psi_a)$'s are bounded by ± 1, we cannot treat $h_{\vec{k}}$'s and $c_{\vec{k}}^a$'s as independent variables to minimize $E_{\rm tot}$. Therefore, we minimize $E_{\rm tot}$ over the orbital variables θ_i at fixed hole configurations; the ground state is then the hole configuration of the lowest energy.

For $La_{7/8}Sr_{1/8}MnO_3$, we consider the three hole configurations shown in Fig. 1, each of which is a Bravais lattice, with a unit cell containing one Mn site with a hole and seven Mn sites without holes. The orbital configuration may be different in different unit cells of the lattice defined by the holes. We consider the case where the orbital configuration is the same in each unit cell. In addition to that, we also con-

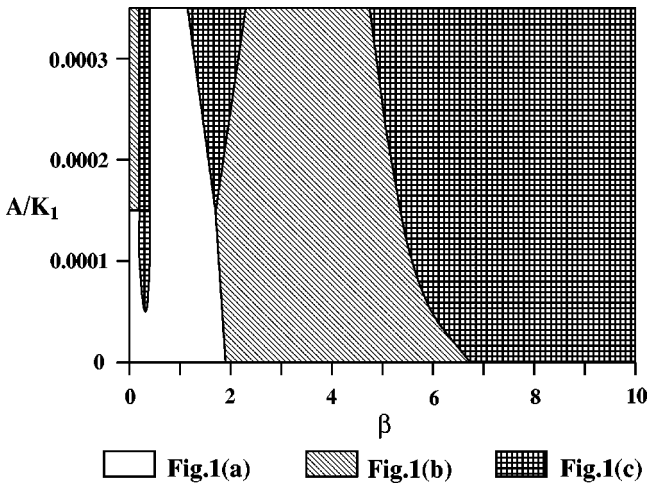

FIG. 3. Phase diagram in the A/K_1 versus β plane for $R_{7/8}A_{1/7}MnO_3$. $\lambda/K_1=0.045$, $K_2/K_1=0.5$, and $g=0$.

sider all possible two sublattice symmetry breakings. Therefore, we have seven (if there is no symmetry breaking) or fourteen (if there is two-sublattice symmetry breaking) orbital variables θ_i. $E_{\rm tot}/N$ in Eq. (17) for each configuration is expressed in terms of those variables through Eqs. (11), (15), (16), (18), and (19) and is minimized about θ_i's. For this minimization, we use the FINDMINIMUM routine in MATHEMATICA in the following way: For each set of parameters and for each configuration, we check the local minimal values by using 50–200 random starting values of θ_i.

According to Ref. 10, λ/K_1 ranges over 0.04–0.05 and K_2/K_1 is between 0 and 1. A/K_1 ranges around 0.0002 and $K_1\approx 200$ eV.[10] Recently, a local breathing distortion of 0.12 Å has been directly observed in $La_{0.75}Ca_{0.25}MnO_3$.[11] The Jahn-Teller distortion is estimated around 0.15 Å from the Mn-O distances of $LaMnO_3$.[12] This implies that the breathing distortion and the Jahn-Teller distortion in these materials have similar orders of magnitude, i.e., $\beta=O(1)$. We varied β in the range 0–10 and A/K_1 in the range 0–0.000 35, with $\lambda/K_1=0.045$, $K_2/K_1=0.5$, and $K_1=200$ eV. For each set of those parameters, the minimum energy per hole for each fixed hole configuration in Fig. 1 has been found. By comparing them, we find the most favored hole configuration for each β and A/K_1, which is shown in Fig. 3 as a plot in $\beta-A/K_1$ plane.

At large $\beta(\gtrsim 7)$, the configuration shown in Fig. 1(c) is the most favored and that shown in Fig. 1(a) is the least favored. This can be related to the fact that, in $y-z$ and $z-x$ directional planes, Fig. 1(c) has the most even distribution of holes and Fig. 1(a) has the least even distribution. For large β, the contraction of oxygen octahedra toward holes is strong and an uneven distribution of holes generates larger strains and elevates minimum energies. In particular, the square hole net squeezes the electron orbital at the center of the square along the direction perpendicular to the square plane. In the cubic hole configuration of Fig. 1(a), the six squeezed electron orbitals point toward the cubic center, putting the electron orbital at the center at high energy, which is consistent with our result that Fig. 1(a) has far higher minimum energies than Figs. 1(b) and 1(c) in the large β limit.

As β is decreased into the range 2–5, the favored hole configuration becomes that of Fig. 1(b), which is the experimentally observed hole configuration. We expect that the difference of the energy per hole between the ground state hole configuration and the next lowest energy hole configuration corresponds approximately to the charge ordering temperature. The calculation results indicate that when β is in the range 2.0–2.5 or around 5.0 and $A/K_1=0.0002$, the charge ordering temperature is around 100–200 K, which is consistent with experimental results. As β is decreased further, the most favored hole configuration changes further and the temperature difference scale decreases.

Figure 3 also shows the tendency that the configuration of Fig. 1(c) becomes more favored as A/K_1 increases. We think that this occurs because the anharmonicity energy distorts the oxygen octahedra tetragonally, which can be more easily accommodated by the tetragonal hole configuration of Fig. 1(c).

In Table I we show an example of the orbital states, ionic displacements, and uniform strains corresponding to the minimum energy configuration for Fig. 1(b) when $A/K_1=0.0002$, $\lambda/K_1=0.045$, $K_2/K_1=0.5$, and $\beta=2.5$. The x,y, and z directions are shown in Fig. 1. The nearest Mn-Mn distance is a unit. (n_i^x,n_i^y,n_i^z) is defined in such a way that $(n_i^x,n_i^y,n_i^z)+N_1(2,0,0)+2N_2(0,2,0)+2N_3(1,0,2)$'s and $(n_i^x,n_i^y,n_i^z)+N_1(2,0,0)+(2N_2+1)(0,2,0)+(2N_3+1)\times(1,0,2)$'s, where N_1,N_2, and N_3 are integers, represent the coordinates of the sites indexed by i. $\vec{k}=\vec{0}$ parts of the ionic displacements have been subtracted to find the nonuniform parts of the displacements.

The energy expressions in Eqs. (18) and (19) are adequate for bulk materials. When the material is grown on a substrate as a thin film, generally there is a strain generated by lattice mismatch between the film and the substrate materials. To see the effect of this strain, we add a term proportional to $c_0^{a'}$ ($a'=x,y,$ or z) to the energy, which corresponds to an a' directional strain. Using a parameter g, we replace $\mathcal{E}_{\vec{k}=0}$ in Eq. (19) by the expression

$$\mathcal{E}'_{\vec{k}=0}=-\frac{\lambda^2}{K_1+2K_2}\left[3(\beta h_0)^2+gc_0^{a'}+\sum_a (c_0^a)^2\right]. \quad (23)$$

We repeated similar calculations to find the favored hole configurations for different values of the applied strain, parametrized by g. The applied strain breaks cubic symmetry. Some of the hole configurations also break cubic symmetry. For these cases the energy depends on the relative orientation of the strain and hole symmetry breakings. We consider all possible orientations and find the lowest energy state. We have varied g between -0.4 and 0.4 and β between 0 and 7, with $A/K_1=0.0002$, $\lambda/K_1=0.045$, and $K_2/K_1=0.5$. The results are shown as a phase diagram in the β-g plane in Fig. 4. It shows that the Fig. 1(c) configuration is favored more as $|g|$ increases. This feature can be understood in the following way. For small g's, the leading correction to the minimum energy for each hole configuration is $-\lambda^2 g\widetilde{c_0^a}/(K_1+2K_2)$, where $\widetilde{c_0^a}$ represents $c_0^a|_{g=0}$. Therefore, the configuration that

TABLE I. Coordinates of site i, orbital states, ionic displacements, and uniform strains for the minimum energy configuration of Fig. 1(b), when $A/K_1=0.0002$, $\lambda/K_1=0.045$, $K_2/K_1=0.5$, and $\beta=2.5$.

i	(n_i^x, n_i^y, n_i^z)	θ_i(rad)	$\delta_i^x-\delta_{\tilde{k}=0}^x$	$\delta_i^y-\delta_{\tilde{k}=0}^y$	$\delta_i^z-\delta_{\tilde{k}=0}^z$	$u_i^x-u_{\tilde{k}=0}^x$	$u_i^y-u_{\tilde{k}=0}^y$	$u_i^z-u_{\tilde{k}=0}^z$
1	(0,0,0)	hole site	0	0	0	−0.135	−0.134	−0.159
2	(1,0,0)	1.11	0	0.007	0	0.135	0.007	−0.039
3	(0,1,0)	1.97	0	0	0	0.004	0.134	−0.030
4	(1,1,0)	0.03	0	0	0	−0.004	−0.007	0.047
5	(0,0,1)	0.09	0	−0.005	−0.049	0	−0.023	0.011
6	(1,0,1)	0.09	0	0.005	−0.007	0	−0.009	0.019
7	(0,1,1)	2.74	0	0	0.002	−0.043	0.023	0.037
8	(1,1,1)	1.24	0	0	0.013	0.043	0.009	−0.008
9	(0,2,0)	hole site	0	0	0	−0.135	−0.133	−0.159
10	(1,2,0)	1.11	0	−0.007	0	0.135	−0.013	−0.039
11	(0,3,0)	2.28	0	0	0	−0.036	0.133	0.008
12	(1,3,0)	1.33	0	0	0	0.036	0.013	−0.037
13	(0,2,1)	0.09	0	0.005	−0.049	0	−0.009	0.011
14	(1,2,1)	0.09	0	−0.005	−0.007	0	−0.023	0.019
15	(0,3,1)	1.24	0	0	−0.013	0.043	0.009	−0.047
16	(1,3,1)	2.74	0	0	−0.002	−0.043	0.023	0.030
Uniform strain			$e^{xx}=-0.014$, $e^{yy}=-0.019$, $e^{zz}=-0.009$					

has a larger $|\widetilde{c_0^a}|$ will show greater change in energy for a given g. Since the hole configuration in Fig. 1(c) has tetragonal symmetry, which is compatible with the Jahn–Teller distortion, it has the largest $|\widetilde{c_0^a}|$. Therefore, as $|g|$ increases, Fig. 1(c) is more favored than Figs. 1(a) and 1(b). Because the energy changes linearly with g, the phase boundaries are straight lines for small g and have cusps at $g=0$, as shown in Fig. 4. Typical variations of e^{aa} corresponding to changing $|g|$ from 0 to 0.4 are about 2%. The results indicate that the strain generated by substrates can change the ordered hole configuration and ordering temperature. Our results indicate that the interaction of the electronic state and the lattice can be the origin of the charge ordering in this material, even though the details of the results are dependent on specific choice of K_1, K_2, λ, and A.

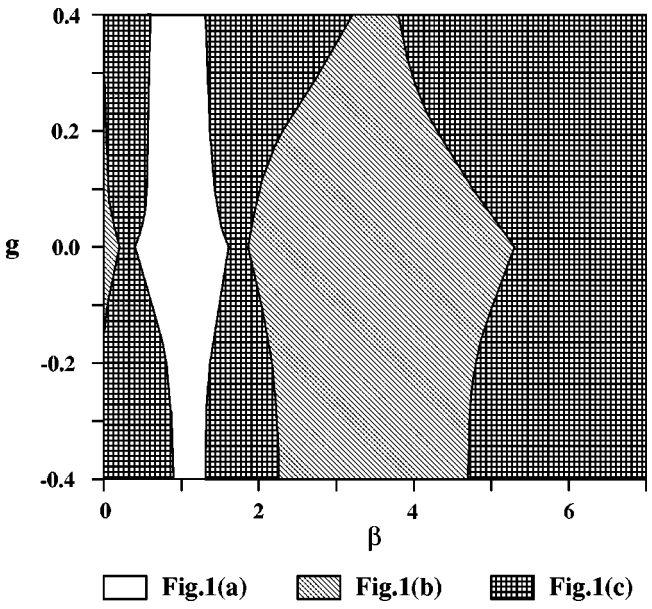

FIG. 4. Phase diagram in the g versus β plane for $R_{7/8}A_{1/7}MnO_3$. $\lambda/K_1=0.045$, $K_2/K_1=0.5$, and $A/K_1=0.0002$.

A similar calculation has been done for $R_{1/2}A_{1/2}MnO_3$, hole concentration 1/2. We choose the three hole configurations in Fig. 5 to compare the minimum energies. Each configuration has an alternating hole distribution in a different set of directions: the x,y, and z directions for Fig. 5(a), the x and y directions for Fig. 5(b), and the y direction for Fig. 5(c). Figure 5(b) is the experimentally observed hole configuration.[2] As we have done for $x=1/8$, we consider both the case where hole and orbital state have the same unit cell and the case where the orbital state is composed of the two hole sublattices. Calculations for $A/K_1=0.0002$, $\lambda/K_1=0.045$, and $K_2/K_1=0.5$ show that when β is large, the configuration in Fig. 5(a) is the most favored and Fig. 5(c) is the least favored. As β is decreased, the favored configuration is changed between $\beta=0.5$ and 0.7. After that Fig. 5(c) is the most favored and Fig. 5(a) is the least favored. When β is large, the holes tend to distribute evenly for the same reason as in the $x=1/8$ case. In contrast, when β is small, electron sites tend to have more neighboring electron sites to gain orbital energy. Our results are not consistent with the experimental results for $La_{1/2}Ca_{1/2}MnO_3$,[2] which indicate that the configuration in Fig. 5(b) is the ground state. This

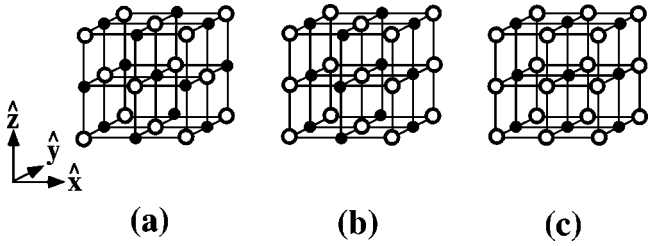

FIG. 5. Three hole ordering patterns for $R_{1/2}A_{1/2}MnO_3$ considered in our calculations. Solid circles represent Mn^{3+} and open circles Mn^{4+}.

inconsistency may arise because our model involves only localized electrons, while for $x=1/2$ the charge ordering state arises from a metallic phase. Modifications of our model to include hole hopping are desirable.

In summary, we have shown that the lattice effect could play an important role in the charge ordering transition observed in perovskite manganites.

Note added in proof. We have discovered an error in Ref. 10; correcting it leads to larger estimates for the anharmonicity parameter. The theoretical results of the present paper are not affected, but the larger anharmonicity reduces the parameter window in which the model reproduces the experimentally observed hole configuration. Further details will be presented elsewhere.

This work was supported in part by NSF Grant No. DMR-9705482. We also acknowledge partial support from NSF Grant No. DMR-96322526 (Johns Hopkins MRSEC for Nanostructured Materials).

APPENDIX

To find the minimum energy we transform $E_{\rm tot}$ in Eq. (12) into $\vec{k}$ space, using Eqs. (13)–(16). This leads to the following energy expressions in k space:

$$E_{\rm tot}/NK_1=\sum_{\vec{k}}\ \delta_{\vec{k}}^{\dagger}M_{\vec{k}}\delta_{\vec{k}}+\delta_{\vec{k}}^{\dagger}L_{\vec{k}}^{\dagger}u_{\vec{k}}+u_{\vec{k}}^{\dagger}L_{\vec{k}}\delta_{\vec{k}}+u_{\vec{k}}^{\dagger}u_{\vec{k}}+u_{\vec{k}}^{\dagger}P_{\vec{k}}e_{\vec{k}}$$
$$+e_{\vec{k}}^{\dagger}P_{\vec{k}}^{\dagger}u_{\vec{k}}-\frac{A}{NK_1}\sum_i\ (1-h_i)\cos 6\theta_i\,, \qquad \text{(A1)}$$

where

$$\delta_{\vec{k}}^{\dagger}=(\delta_{\vec{k}}^{x},\delta_{\vec{k}}^{y},\delta_{\vec{k}}^{z}), \qquad \text{(A2)}$$

$$u_{\vec{k}}^{\dagger}=(u_{\vec{k}}^{x},u_{\vec{k}}^{y},u_{\vec{k}}^{z}), \qquad \text{(A3)}$$

$$e_{\vec{k}}^{\dagger}=(\beta h_{\vec{k}}-c_{\vec{k}}^{x},\beta h_{\vec{k}}-c_{\vec{k}}^{y},\beta h_{\vec{k}}-c_{\vec{k}}^{z}), \qquad \text{(A4)}$$

$$M_{\vec{k}}=\begin{pmatrix} 1+\frac{K_2}{K_1}(1-\cos k_x)+\frac{K_3}{K_1}(1-\cos k_x\cos k_y)+\frac{K_3}{K_1}(1-\cos k_x\cos k_z) & \frac{K_3}{K_1}\sin k_x\sin k_y & \frac{K_3}{K_1}\sin k_x\sin k_z \\ \frac{K_3}{K_1}\sin k_y\sin k_x & 1+\frac{K_2}{K_1}(1-\cos k_y)+\frac{K_3}{K_1}(1-\cos k_y\cos k_z)+\frac{K_3}{K_1}(1-\cos k_y\cos k_x) & \frac{K_3}{K_1}\sin k_y\sin k_z \\ \frac{K_3}{K_1}\sin k_z\sin k_x & \frac{K_3}{K_1}\sin k_z\sin k_y & 1+\frac{K_2}{K_1}(1-\cos k_z)+\frac{K_3}{K_1}(1-\cos k_z\cos k_x)+\frac{K_3}{K_1}(1-\cos k_z\cos k_y) \end{pmatrix}, \qquad \text{(A5)}$$

$$L_{\vec{k}}=\begin{pmatrix} -\frac{1}{2}(1+e^{ik_x}) & 0 & 0 \\ 0 & -\frac{1}{2}(1+e^{ik_y}) & 0 \\ 0 & 0 & -\frac{1}{2}(1+e^{ik_z}) \end{pmatrix}, \qquad \text{(A6)}$$

$$P_{\vec{k}}=\frac{\lambda}{2K_1}\begin{pmatrix} 1-e^{ik_x} & 0 & 0 \\ 0 & 1-e^{ik_y} & 0 \\ 0 & 0 & 1-e^{ik_z} \end{pmatrix}, \tag{A7}$$

and N is the total number of Mn sites. We obtain Eqs. (18)–(22) by minimizing the above expression with respect to all $\delta^a_{\vec{k}}$ and $u^a_{\vec{k}}$. Without the second neighbor elastic energy term, $\delta_{\vec{k}}$ and $u_{\vec{k}}$ minimizing Eq. (A1) become singular when any of k_x, k_y, and k_z is zero. With nonzero K_3 this singularity has been uniquely solved for $\vec{k}\neq\vec{0}$, while at $\vec{k}=\vec{0}$ it is not.

To find the energy term with $\vec{k}=\vec{0}$, we take the $\vec{k}\to\vec{0}$ limit. That corresponds to the uniform strain energy, i.e., the energy related to the change of the lattice parameters from the original cubic structure. Here the problem of the choice of the limiting process arises because the calculation shows that the different directions of the limiting process of $\vec{k}\to\vec{0}$ have given different energies and different uniform strains. Because the lower energy state is favored after all, the appropriate limiting process will be the one that gives the minimum uniform strain energy and it determines the uniform strain also. When $K_3/K_1 \ll 1$, this appropriate limiting process has been found to satisfy the condition of k_x, k_y, and $k_z \neq 0$. As long as k_x, k_y, and k_z are nonzero, the limits are different only on the order of K_3/K_1. Therefore, in the $K_3/K_1 \to 0$ limit, any $\vec{k}\to\vec{0}$ limit process satisfying the above condition gives the correct expression of the minimum energy term with $\vec{k}=\vec{0}$. It also gives a unique uniform strain.

[1] R. von Helmolt, J. Wecker, B. Holzapfel, L. Schultz, and K. Samwer, Phys. Rev. Lett. **71**, 2331 (1993); S. Jin, T. H. Tiefel, M. McCormack, R. A. Fastnacht, R. Ramesh, and L. H. Chen, Science **264**, 413 (1994); K. Liu, X. W. Wu, K. H. Ahn, T. Sulchek, C. L. Chien, and J. Q. Xiao, Phys. Rev. B **54**, 3007 (1996).

[2] C. H. Chen and S-W. Cheong, Phys. Rev. Lett. **76**, 4042 (1996).

[3] Y. Murakami, H. Kawada, H. Kawata, M. Tanaka, T. Arima, Y. Moritomo, and Y. Tokura, Phys. Rev. Lett. **80**, 1932 (1998).

[4] Y. Yamada, O. Hino, S. Nohdo, R. Kano, T. Inani, and S. Katano, Phys. Rev. Lett. **77**, 904 (1996).

[5] Y. Okimoto, T. Katsufuji, T. Ishikawa, T. Arima, and Y. Tokura, Phys. Rev. B **55**, 4206 (1997).

[6] N. W. Aschcroft and N. D. Mermin, *Solid State Physics* (Saunders College Publishing, Fort Worth, 1976).

[7] H. Kawano, R. Kajimoto, M. Kubota, and H. Yoshizawa, Phys. Rev. B **53**, 2202 (1996); **53**, 14 709 (1996).

[8] E. O. Wollan and W. C. Koehler, Phys. Rev. **100**, 545 (1955).

[9] J. Kanamori, J. Appl. Phys. **31**, 14S (1960).

[10] A. J. Millis, Phys. Rev. B **53**, 8434 (1996).

[11] S. J. L. Billinge, R. G. DiFrancesco, G. H. Kwei, J. J. Neumeier, and J. D. Thompson, Phys. Rev. Lett. **77**, 715 (1996).

[12] J. B. A. A. Ellemans, B. van Laar, K. R. van der Veen, and B. O. Loopstra, J. Solid State Chem. **3**, 238 (1971).